Stick-Slip Phenomena in Dynamics: choice of contact model

Eric Chatelet, Guilhem Michon, Lionel Manin, Georges Jacquet-Richardet

Stick/Slip Phenomena in Dynamics: Choice of Contact Model. Numerical Predictions & Experiments

E. Chatelet*, G. Michon†, L. Manin‡, G. Jacquet§
LaMCoS, INSA-Lyon
CNRS UMR5259**,** F69621, France

Abstract— This paper presents a method for choosing the most appropriate contact model from several models, by comparing their efficiency for predicting hysteretic behaviour in different applications. The first part describes an application for a belt tensioner used for automotive engines. The second part concerns an academic application and focuses on a simple case of vibration in the presence of dry friction. The hysteresis loops obtained at contact locations are usually used to reproduce the nonlinear forces transmitted along the contact surface as accurately as possible. Although such techniques can be used when the contact zone is easily accessible, this is not generally possible for real, complex structures. Consequently, different techniques are developed and validated.

Keywords: stick/slip contact, hysteresis loop, macro/microslip, nonlinear

I. Introduction

One of the most common failure modes for mechanical components is high-cycle fatigue. To avoid high amplitudes and extend the working life of machines, natural frequencies have to be distinguished from excitation frequencies. However, in practice, real structures are characterized by so many natural frequencies that it is impossible to eliminate resonance, while vibratory stresses must to be reduced either by using specific devices (for example, belt tensioners for automotive applications) or by increasing structural damping (friction devices in blade-disc assemblies in turbomachinery).

The objective of this work is to improve understanding and modelling of stick/slip phenomena encountered in different industrial applications. For example, coupling devices (Griffin [1]) are introduced in bladed stages to increase resonance frequencies above the range of possible excitations. They are not only often used to stiffen flexible structures, but also to increase damping by dry friction, thereby reducing the amplitude of vibration.

*E-mail: eric.chatelet@insa-lyon.fr
† E-mail: guilhem.michon@ insa-lyon.fr
‡ E-mail: lionel.manin@ insa-lyon.fr
‡ E-mail: georges.jacquet@ insa-lyon.fr

Likewise, tensioners used in belt drive systems act as passive controllers by maintaining nominal tension in the slack span and reducing transverse vibration levels (Beikmann [2]).

The literature describes many kinds of contact models. Friction devices (Panning et al. [3]) are used in many mechanical applications to decrease vibrational amplitudes and reduce stress levels. Different contact models (Menq [4]), (Mindlin [5]) and (Petrov and Ewins [6]) have been developed to simulate the dynamic behaviour of structures with dry friction effects. The hysteretic behaviour of components allows efficient control of mechanical systems but their significant nonlinearity [7, 8] makes predicting response difficult. Vestroni and Noori in [8] and Visintin in [9] give an overview of hysteresis models.

However, choosing the best adapted contact model for a specific application is far from obvious. Rheological models and restoring force models are the two main categories used in mechanical engineering to predict component behaviour, as described by Michon [10]. The former provide damping and stiffness parameters (see §3), while the latter provide a restoring force to be introduced in the second member of equations. The objective of this work is to prove, via different applications, that different phenomelogical and rheological models can be used successfully when linked with pertinent hypotheses and/or measurements. Therefore analysis of the contact can be "global" and encompass an entire mechanical system or else it can require more precision in order to describe the real phenomena in the contact zone. Firstly, the application of a restoring force model is tested with sufficient accuracy for a belt tensioner automotive system. A second application demonstrates that Frequency Response Functions can be used to facilitate the choice between more dedicated macro or microslip models.

II. A phenomenological model used on an automotive tensioner

Satisfying technological challenges often leads to complicated design solutions for tensioners, and involves considerably nonlinear behaviour mainly due to stick-slip motion, see for example [13, 14].
The modified Dahl model [11, 12], known as the restoring

force model or phenomenological model, is selected for this analysis and used globally, without analyzing the real nature of the contact or dissipation. The modified Dahl model is based on a first differential equation that provides the time derivative of restoring force F from the velocity of deflection u and from the envelope curves of the hysteresis.

$$\frac{dF}{dt} = \beta \frac{du}{dt}\left(h - Fsgn\left(\frac{du}{dt}\right)\right) \quad (1)$$

$$h = \frac{1}{2}\left(\left(h_u + h_l\right)\mathrm{sgn}\left(\frac{du}{dt}\right) + \left(h_u - h_l\right)\right) \quad (2)$$

Parameters β and μ are constants. Functions h_u and h_l define respectively the upper and lower asymptotic equations of the model. These functions depend on many parameters such as forcing frequency, motion amplitude and temperature. An initial experimental set-up is used for identifying the model parameters associated with the global dissipation of the system. Then, a second set-up permits comparing the predicted and measured FRFs in order to discuss the efficiency of the model proposed.

II.1 Description and parameters identification

As illustrated in figure 1, the tensioner is composed of fore parts: Part 1 is a solid (Idler pulley) that rotates around axis $\Delta = (AB)$ of part 2; part 2 is the tensioner arm, ABC, that rotates around the fixed axis Δ' of part 3, which is bolted to the reference part 4 (i.e. an engine for automotive applications). All the parts are considered as rigid bodies. The pin joint of axis Δ' between parts 2 and 3 includes a torsion spring and friction components that cause dry and lubricated contact forces, and a moment between parts 2 and 3. The phenomena involved cause the joint to have highly nonlinear behaviour.

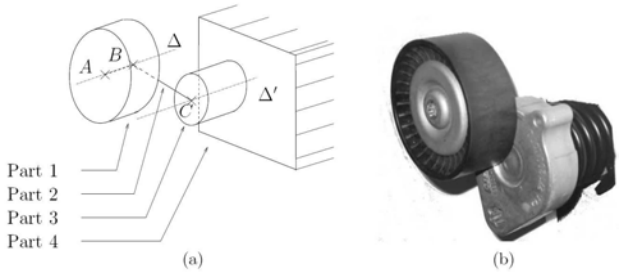

Fig. 1. Tensioner scheme (a) and picture (b).

An experimental set up has been designed to identify the parameters of the belt tensioner model. The idler pulley is removed and segment AB is connected to a rigid bar that subjects a vertical alternative displacement on point A. The vertical components of point A, displacement u(t), and force F are considered positive when oriented toward the ground, since the tensioner is always preloaded when in use. Force F remains positive. The displacements are measured using laser optical sensors, while the forces are measured with load cells. Data acquisition is performed simultaneously at a sampling frequency f_{sto} = 5000 Hz. The measurements can be filtered to remove measurement noise. An alternative vertical displacement is imposed on point A. After a transient state (starting from initial position), a steady hysteretic loop is observed as shown in figure 2 and the measured force F versus time is periodic. In order to identify the parameters defining h_u and h_l, we draw advantage from the fact that h_u and h_l represent the upper and lower envelop curves of the hysteretic loop to which the pair (u(t),F(t)) belongs. By analysing the measured loop shown in figure. 2, the envelop curves h_u and h_l can be considered as straight lines, so the asymptotic equations can be determined by using the mean square approximation method.

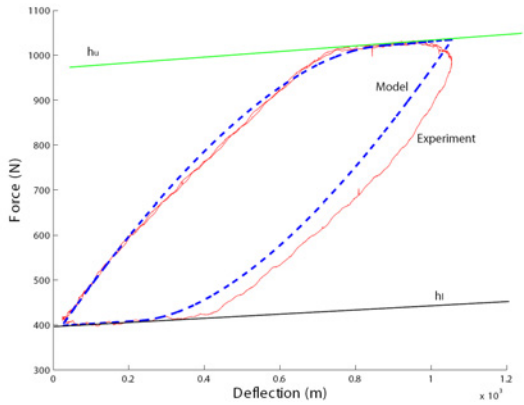

Fig. 2. Force-deflection hysteretic loop for the tensioner: Experiment (-) and model (--). Parameter idenfication of the envelop curves of the model: h_u, h_l..

II.2. Dynamic system

In the previous section, the Modified Dahl model was formulated for the belt tensioner. The tensioner is now a part of a mechanical system subjected to a variable load excitation. The purpose is to test the model's efficiency by considering a multi-degree of freedom system and performing an experimental investigation. The tensioner model is implemented in the system motion equations that are solved numerically. The predicted and measured results are compared.

The dynamic system considered is composed of the previously studied tensioner, a poly-V belt and a mass (see figure 3). The tensioner base is fixed on a rigid frame. Its idler pulley of mass m_2 has a belt wound around it. The two adjacent belt spans are joined at their ends and connected to mass m_1. Mass m_1 is excited by the imposed force f generated by an electro-dynamic shaker (see figure. 3). Two displacements u_1 and u_2 of the two masses

are measured with laser-optical displacement sensors. The transmitted force f is measured with a piezo-electric load sensor and the belt tension is measured with an S-shape load sensor. In this two degree of freedom system, mass m_1 is used both for tensioner preload and for system dynamics

Equations of motion:

Let u_1 and u_2 be the vertical displacements of masses 1 and 2 along the x axis; they are both positive and oriented downward. F is the force exerted by the tensioner on the pulley, it is positive, oriented upward and modeled using the previously identified Modified Dahl model. Force f is positive and oriented downward. Let $T/2$ be the tension in each belt span. Due to the ratio between the radius of the pulley and the belt span lengths, it is assumed that tension T is oriented vertically.

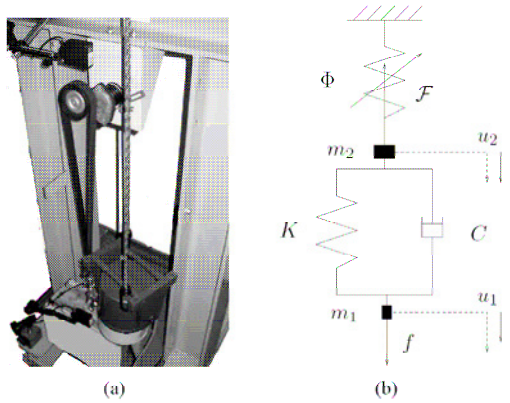

Fig. 3. Dynamic system and model

By considering the belt as a spring-damper of stiffness K and equivalent viscous damping C, the belt behaviour law is defined by:

$$T(t) = K\left(u_1 - u_2\right) + C\left(\frac{du_1}{dt} - \frac{du_2}{dt}\right) + T_0 \quad (3)$$

By neglecting effects on the horizontal axis, the dynamic equilibrium of the tensioner pulley projected along the vertical axis x leads to the following nonlinear equation:

$$m_2 \frac{d^2u_2}{dt^2} = T(t) - F(t) + m_2 g \quad (4)$$

By neglecting effects on the horizontal axis, the dynamic equilibrium of the lower mass projected along the vertical axis x leads to:

$$m_1 \frac{d^2u_1}{dt^2} = -T(t) + f(t) + m_1 g \quad (5)$$

II.3 Results: Global behaviour FRF

The amplitude |max(T) − min(T)| versus forcing pulsation are measured for several values of f. Measured and predicted responses are plotted in figures 4 and 5. The computed frequency response represented in these figures is obtained after a series of calculations in the time domain: each point of a frequency response curve corresponds to the amplitude of belt tension fluctuation calculated when steady state is reached for a given frequency and excitation amplitude. The dot-dashed curves correspond to the predicted results obtained for higher excitation force amplitudes not obtained experimentally due to set-up limitations. Experimental observations show that even if the excitation force amplitude increases, the resulting belt tension variation is bounded within a frequency range.

This phenomenon is well predicted and proves the efficiency of the modified Dahl model for such an application. The system's behaviour, shown in figure 5, is similar to that described in [16, 17]. The tensioner sticks for low forcing amplitudes, but mostly slips for high forcing amplitudes.

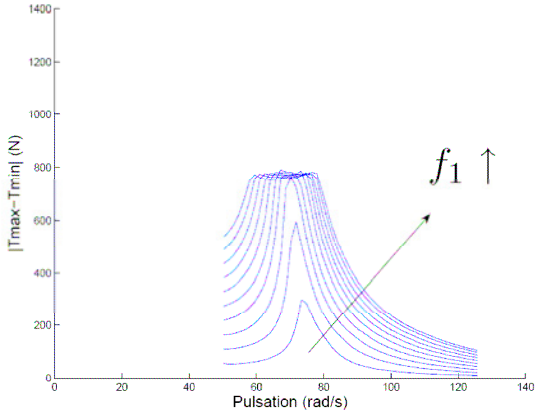

Fig. 4. Global behaviour of the dynamic system: Experimental FRF

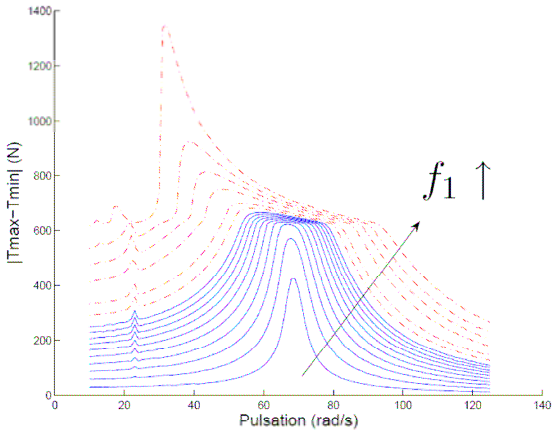

Fig. 5. Global behaviour of the dynamic system: Restoring force model FRF

In conclusion, we can see that this restoring force model is suitable for a dissipative mechanical system, and not limited to only dry friction. Nevertheless, it requires

measurements under harmonic excitation. One main drawback is that the parameters identified have no physical significance. Unfortunately, although such techniques may be used when the contact zone is easily accessible, this is generally not possible for real, complex structures used in turbomachinery. Therefore more sophisticated models have to be employed, with respect to the real nature and behaviour of the contact zone.

III. Rheological model: vibration analysis of a cantilever beam with a dry friction contact in an academic application

Rheological models can be divided into two categories: macroslip and microslip models according to the homogeneity of contact states, as observed by D'Ambrosio [15, 16]. Briefly, for stick/slip contact states, the hysteresis loops are represented by a perfect parallelogram when associated with macroslip cases (stuck contact stiffness remains constant) and by a curved parallelogram when associated with microslip cases (stuck contact stiffness is no longer straight and the slope of the hysteresis loop decreases). The macroslip model allows dissipation only when the whole surface slips.

Recent experimental applications (Sextro [17]) confirm that roughness may have an important influence on the identification of contact parameters. For low normal loads, adherence between contact surfaces is imperfect because of roughness. Consequently, the real contact surface or equivalent contact stiffness is lower than the asymptotic value reached when the roughness is completely worn (obtained in the case of very high normal loads).

For real complex industrial structures, it is not always possible to carry out an experimental approach (Toufine et al. [18]), making it is necessary to seek different techniques. Here, a numerical analysis based on a single degree of freedom system is used to point out the main differences between the Frequency Response Functions (FRFs) obtained from different contact models (macroslip, microslip with and without roughness effect). After analysis of the different dynamic behaviours obtained, a criterion is proposed in order to choose the most appropriate contact model directly from the FRFs, without performing any experimental hysteresis loop analysis. Finally, an experimental / numerical study of a cantilever beam with dry friction effects is performed in order to validate the proposed approach.

III.1 Dynamic behaviour with macroslip and microslip models without roughness effects

A single dof system (figure 6) is used to show the influence of the contact model on dynamic behaviour. For such systems, the motion equation is:

$$m\ddot{x}_t + c\dot{x}_t + kx_t = F_{ex}\cos(\omega t) - \mathrm{f_t} \qquad (6)$$

with m being mass, k stiffness, c viscous damping, F_{ex} amplitude of the excitation force (ω pulsation) and $\mathrm{f_t}$ nonlinear force at the contact. The classical Harmonic Balance Method (Masiani et al. [19]) is used to solve the nonlinear equation in the frequency domain and obtain results faster than in the time domain.

The FRFs obtained from a Masing macroslip model are reported in figure 7. Two resonance peaks are present: the first at high frequency is associated with a fully stuck case obtained when the ratio between the excitation force and the normal load is very low (F_{ex}/F_n=0.001), while the second, associated with the case in full slip state, is obtained when this ratio is high (F_{ex}/F_n=10).

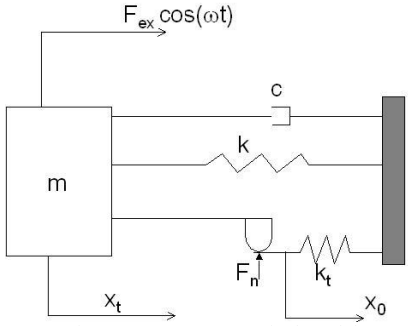

Fig. 6. One DOF numerical model

For intermediate F_{ex}/F_n values, the contact state is stick/slip and the associated dynamic behaviour is strongly nonlinear with a classical peak flattening characteristic.

Moreover, for F_{ex}/F_n ratios <0.2 the contact is stick/slip with a majority stuck and the FRFs flatten in conformity with the fully stuck peak, but also remain within the envelope curve of the fully stuck case. The same numerical results may be obtained for different values of excitation forces or normal loads but in every case, the FRFs depend only on the ratio F_{ex}/F_n ratio.

With a microslip model, two different resonance peaks are also associated with the fully stuck and full slip states, obtained respectively for F_{ex}/F_n=0.001 and F_{ex}/F_n=10.

As for the macroslip case, a nonlinear dynamic behaviour is associated with stick/slip contact states for intermediate values of F_{ex}/F_n (figure 8). However, here, the FRFs associated with stick/slip states when most of the contact remains stuck do not belong to the envelope curve of the completely stuck response, but move toward lower frequencies. This displacement of FRFs is a function of the amount of slipping at the edges of the contact surface while the rest of the surface remains stuck.

This phenomenon depends exclusively on the presence of different contact states along the contact surface, thus other microslip models (Sanliturk and Ewins [20]) produce the same behaviour with a translation of FRFs to the left. Whatever the case, for microslip and macroslip models, FRFs depend exclusively on the ratio between excitation force and normal load and, consequently, the

only possible difference is due to the small displacement of the maximal amplitude peaks in a microslip case for a mostly stuck stick/slip contact state.

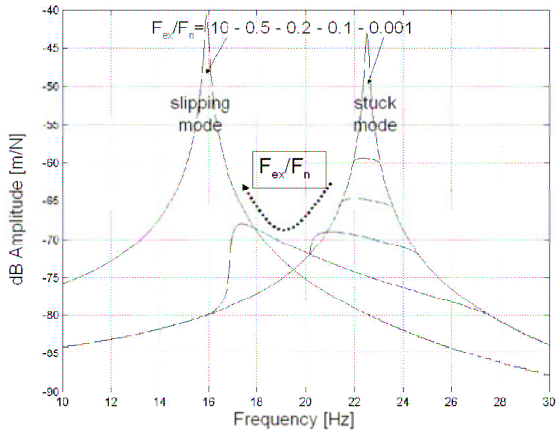

Fig. 7. FRFs for Masing macroslip model

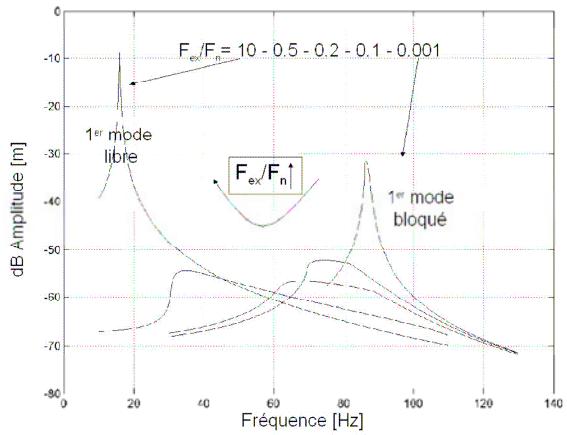

Fig. 8. FRF's for a Menq microslip model

The effects of roughness are now considered for macroslip and microslip models and two different values of the excitation force (F_{ex} = 1 and 1000 N). The same values of contact properties considered in(Sextro [17]) have been used. For the macroslip case when F_{ex} = 1000 N, the tangential stiffness reaches its asymptotic value because normal loads are higher than the normal limit load at 300 N (F_n = 5e3 - 1e4 - 1e6 N). For F_{ex}/F_n ratios = 10 - 0.5 - 0.2 - 0.1 - 0.001, the dynamic behaviour obtained is identical to the behaviour associated with a "pure" macroslip case without roughness effects. The FRFs are identical to those shown in figure 7. When the normal load is 100 N (then for F_{ex}/F_n= 10), the value of the tangential stiffness decreases and the global behaviour of the contact is in full slip state.. Consequently, tangential stiffness has no influence on the FRF. Thus for very high levels of excitation force and normal load, the influence of roughness is negligible and dynamic behaviour is globally identical to that obtained in the case of "pure" macroslip.

However, the dynamic behaviour is quite different when the excitation force is F_{ex} = 1N. Considering the same ratios of F_{ex}/F_n, normal loads are very low (F_n=0.1–2-5-10 N); consequently, the contact surface is not completely adhesive and the tangential stiffness is lower than its asymptotic value. The main consequence is that FRFs translate toward lower frequencies (figure 9). Then, when the adherence of the contact surface is not perfect because of roughness effects, a displacement is observed toward lower frequencies of the FRF and, consequently, FRFs are no more a unique function of the F_{ex}/F_n ratio (see figures 7 and 9).

The same conclusions may be drawn for microslip models. Low normal loads do not produce fully adherent surfaces and the value of the nominal contact area is lower than the asymptotic value.

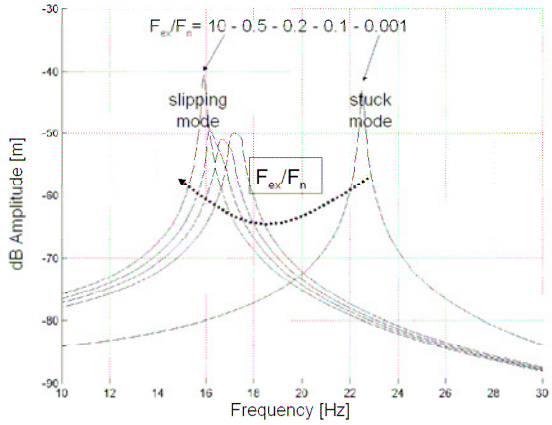

Fig. 9. Effects of roughness on FRFs for a Masing macroslip model

The same values of F_{ex}/F_n as those used for the macroslip analysis are considered here.

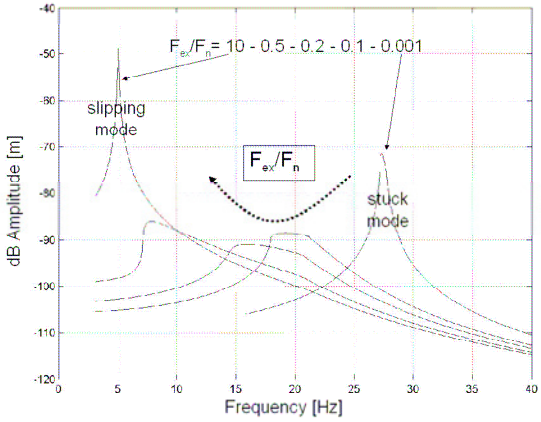

Fig. 10. Effects of roughness on FRFs for a Menq microslip model

When the excitation force is very high (F_{ex} = 1000 N), there is no difference in comparison to a "pure" microslip case because the normal load is sufficient to crush the surface roughness. The contact surface is fully adherent and the FRFs are identical to those shown in figure 8.

When the excitation force is F_{ex} =1N, the roughness effects are very significant (figure 10), and the displacement of maximal amplitude peaks toward lower frequencies, is stronger than in the case of a ”pure” microslip. In conclusion, a criterion is proposed to permit choosing an adapted contact model on the basis of an analysis of dynamic behaviour. If the FRFs depend only on the F_{ex}/F_n ratio, then a ”pure” microslip or a ”pure” macroslip contact model can be selected. In the case of a mostly stuck stick/slip contact state, if the maximal amplitude peak moves towards lower frequencies, the best-adapted model is microslip. On the contrary, if the dynamic behaviour is not the unique function of the F_{ex}/F_n ratio, the roughness effects cannot be neglected. An analysis at very high levels of normal load can be performed in order to crush the surface peaks and establish the adherence between the contact surfaces. In this case, if the maximal amplitude peak still moves toward lower frequencies, the best contact model is microslip with roughness effects. If this is not the case then a macroslip model with roughness effects should be chosen.

III.2 Combined Experimental/Numerical Validation

To validate the proposed method, a simple experimental analysis considering a cantilever beam in the presence of dry friction was performed. Displacements of maximal amplitude peaks in a stick/slip contact state and the influence of the F_{ex}/F_n ratio on the FRFs were analysed to determine the most appropriate contact model.

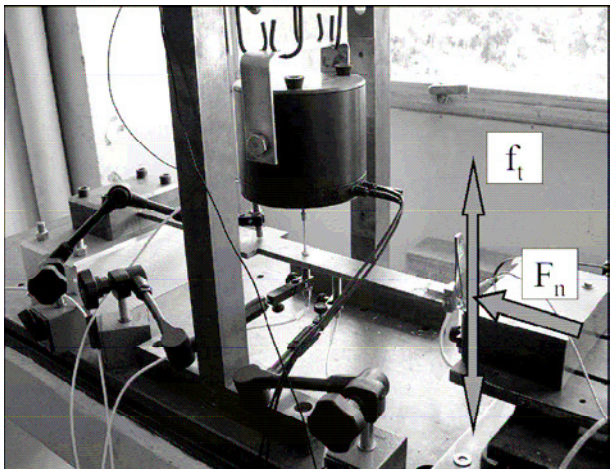

Fig. 11. Experimental Set up

A cantilever beam 0.50 m in length, with a rectangular cross section of 0.008 m by 0.04 m linked with a rubbing element at its free end was considered (figure 11) and instrumented with four eddy sensors. The FRFs measured (figure 12) show the influence of normal load on the dynamic behaviour. More specifically, when the normal load was very high (F_n = 40 N) in comparison with the excitation force (F_{ex} = 2 N), the dynamic behaviour was linear and the FRF reached a resonance peak of 87 Hz. For lower normal loads, the FRFs became flat and the maximal amplitude peak disappeared completely when the normal load was equal to 1 N. Finally, when the normal load was much lower (F_n = 0.5 N) than the excitation force, the contact was in full slip state while the dynamic behaviour was linear with a lower resonance frequency (24 Hz). It clearly appears that the FRFs belonged to the same envelope curve associated with the completely stuck case.

This first characteristic implies that a macroslip contact model should be adapted to reproduce the dynamic behaviour of the structure. Moreover, an analysis considering the influence of the F_{ex}/F_n ratio was performed to verify roughness effects.

Three different F_{ex}/F_n ratios were considered: 0.5, 1 and 2. Each of these ratios were obtained from various values of normal loads, such as 2.5 - 3 - 5 - 10 N.

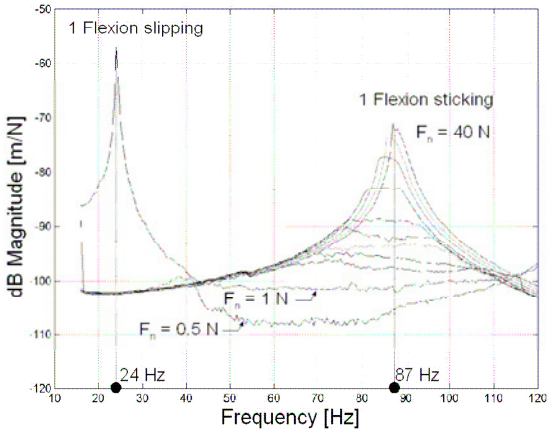

Fig. 12. Measured FRF’s

Figure 13 gives the FRFs associated with the first sensor and obtained from the 12 tested configurations. These results show that response levels can reasonably be considered as being dependent only upon the F_{ex}/F_n ratio. In conclusion, the FRFs lie within the same envelope of the fully stuck case and they depend only upon the F_{ex}/F_n ratio. Consequently, according to the criterion, a macroslip model without roughness effects can be considered for numerical applications. The whole structure was modeled using 13 beam elements (2 nodes with 3 dof for a total of about 40 dof). A frequency domain solution method (HBM) was chosen in order to obtain a good experimental / numerical comparison (figure 14) and validate the proposed approach.

Here, a criterion adapted to the choice of contact models based on an analysis of FRFs has been proposed and validated experimentally. The influence of different contact models (macroslip - microslip models with and without roughness effects) on the dynamic behaviour has been illustrated using a single dof system. The choice of the most appropriate contact model is based on the

properties associated with the influence of F_{ex}/F_n ratio and with the displacement of the maximal amplitude peaks toward lower frequencies. Finally, the proposed criterion was validated by a very good experimental / numerical fit, demonstrating the possibility of choosing contact models by only considering FRFs, without any experimental analysis of hysteresis loops.

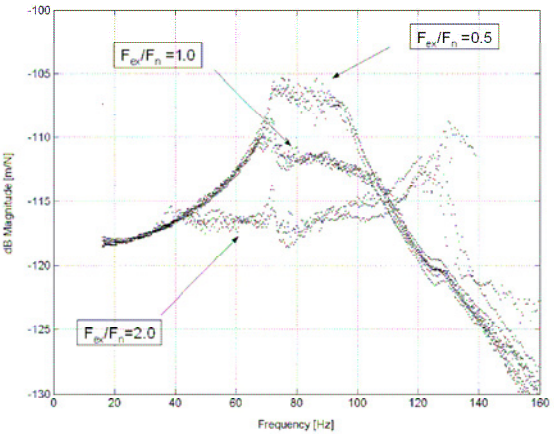

Fig. 13. Measured FRF's

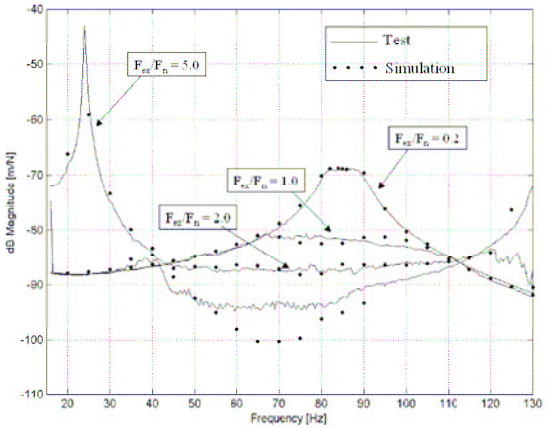

Fig. 14. Experimental/numerical correlations

V. Conclusion

Consequently, this study succeeded in demonstrating that different techniques can be used to describe stick/slip phenomena in industrial mechanisms. Modeling the dynamic behaviour of structures in the presence of dry friction and stick-slip phenomena was considered by using 2 spatial scales, i.e.

- That of a phenomenological analysis capable of examining complicated systems and applicable to other types of specific behaviour, e.g. viscoelastic,
- That of rheological analysis which provides more in-depth examination of the contact state by using the macroslip and microslip approaches. This analysis incorporates tribological considerations such as roughness and wear.

References

[1] Griffin J.H.: 1990, "A review of friction damping of turbine blade vibration," International Journal of Turbo and Jet Engines, 7, pp. 297-307.

[2] R.S. Beikmann, N.C. Perkins, and A.G. Ulsoy. Design and analysis of automotive belt drive systems for steady state performance. ASME Journal of Mechanical Design, 119:162–168, 1997.

[3] Panning L. Sextro W. Popp K.: 2000, "Optimisation of interblade friction damper design," Proc. of the 2000 ASME Turbo Expo, Munich, Germany, ASME Paper GT-2000-541.

[4] Menq C.H.: 1985, "The vibratory response of frictionally constrained gas turbine engine blades," Ph. D. thesis Carnegie - Mellon University Pittsburgh, Pennsylvania.

[5] Mindlin, R. (1949). Compliance of elastic bodies in contact. Journal of Applied Mechanics 16, 259–268.

[6] Petrov, E. and D. Ewins (2002). Analytical formulation of friction interface elements for analysis of nonlinear multi-harmonic vibrations of bladed disc. Proceedings of ASME Turbo Expo, Amsterdam,The Netherlands, June 3-6, 2002.

[7] W. Lacarbonara and F. Vestroni. Non classical responses of oscillators with hysteresis. Nonlinear Dynamics, 32:235, 2003.

[8] F. Vestroni and M. Noori. Hysteresis in mechanical systems - modeling and dynamic response. International Journal of Non-Linear Mechanics, 37:1261–1262, 2002.

[9] A. Visintin. Differential models of hysteresis. Springer-Verlag, Berlin, 1994.

[10] G. Michon, L. Manin, and R. Dufour. Hysteretic behaviour of a belt tensioner: Modeling and Experimental investigation. Journal of Vibration and Control, 11(9):1147–1158, 2005.

[11] A. Al Majid and R. Dufour. Formulation of a hysteretic restoring force model. Application to vibration isolation. Nonlinear Dynamics, 27:69–85, 2002.

[12] A. Al Majid and R. Dufour. Harmonic response of a structure mounted on an isolator modelled with a hysteretic operator: Experiment and prediction. Journal of Sound and Vibration, 277:391–403, 2004.

[13] R.G. Parker. Efficient eigensolution, dynamic response, and eigensensitivity of serpentine belt drives. Journal of Sound and Vibration, 270:15–38, 2004.

[14] M.J. Leamy and N.C. Perkins. Nonlinear periodic response of engine accessory drives with dry friction tensioners. ASME Journal of Vibration and Acoustics, 120:909–916, 1998.

[15] D'Ambrosio F. , Chatelet E. , Ravoux J., Jacquet-Richardet G., " Forced Response of Shrouded Bladed Disc Assemblies: A Jointed Experimental Numerical Approach", Proceedings of ASME Turbo Expo 2004, Power for Land, Sea and Air, IGTI 2004, Vienna Austria, 14-17 juin 2004., GT-2004-53705.

[16] D'Ambrosio F. , Chatelet E., Jacquet-Richardet G., " Influence of contact states on the dynamic behaviour of rubbing structures", Proceedings of ASME Turbo Expo 2005, Power for Land, Sea and Air, IGTI 2005, Reno-Tahoe, Nevada USA,, 06-09 June 2005, GT-2005-68560.

[17] SextroW.: 2000, "The calculation of the forced response of shrouded blades with friction contact and its experimental verification," Proc.of the 2000 ASME Turbo Expo International Gas Turbine & Aeroengine Congress & Exhipition May 8-11, Munich, Germany, ASME Paper 2000-GT-540.

[18] Toufine A., Barrau J.J., Berthillier M.: 1999, "Dynamic study of a structure with flexion-torsion coupling in the presence of dry friction," Nonlinear Dynamics, 18, pp. 321-337.

[19] Masiani, R., D. Capecchi, and F. Vestroni (2002). Resonant and coupled response of hysteretic two-degree-of freedom using harmonic balance method. International Journal of Non-Linear Mechanics 37, 1421–1434.

[20] Sanliturk, K. and D. Ewins (1996). Modelling two dimensional friction contact and its application using harmonic balance method. Journal of Sound and Vibration 206, 39–60.